High-Speed Optical Imaging of Afferent Flow through Rat Olfactory Bulb Slices: Voltage-Sensitive Dye Signals Reveal Periglomerular Cell Activity

David M. Senseman

Division of Life Sciences, The University of Texas at San Antonio, San Antonio, Texas 78249

Fast, multiple-site optical recording and video imaging techniques were combined to visualize the olfactory processing stream as it flowed through rat olfactory bulb slices stained with the voltage-sensitive dye RH155. A 464 element photodiode detector array was used to record the voltage-sensitive dye signals. Focal electrical stimulation of the olfactory nerve layer evoked relatively large optical responses in the olfactory nerve and glomerular layers but only small responses within the external plexiform layer. With paired-pulse stimulation, glomerular attenuation was evident in signals recorded from the glomerular and external plexiform layers but not from the olfactory nerve layer. At very high recording speeds (<0.2 msec/frame), the presynaptic component of the olfactory processing stream could be followed as it flowed through the olfactory nerve layer and into the glomerular layer, where its amplitude rapidly declined. This decline was followed by a reciprocal rise in a postsynaptic depolarization that was largely restricted to the glomerular layer. Spatiotemporal interactions between overlapping afferent streams within the glomerular layer were observed and partially characterized. The optically recorded glomerular layer response was largely resistant to bath application of $GABA_A$ receptor antagonists but was sensitive to manipulations of external chloride concentration and to bath application of a stilbene derivative, 4-acetamido-4′-isothiocyanatostilbene-2,2′-disulfonic acid known to block Cl^- conductances. It is suggested that the voltage-sensitive dye signals recorded from the glomerular layer reflect activity in periglomerular cells and that Cl^- efflux through non-$GABA_A$ chloride channels contributes to the postsynaptic depolarization of these cells after olfactory nerve stimulation.

Key words: olfaction; olfactory bulb; periglomerular cell; optical recording; voltage-sensitive dye; brain slice; chloride; rat

The central mystery of olfaction is how the brain discriminates between different odors. Because primary olfactory receptors show low specificity, it has long been assumed that quality discrimination is linked to differences in the patterns of neural activity evoked in the olfactory bulb and higher centers (Adrian, 1950). One way to examine this hypothesis directly is through the use of voltage-sensitive dyes in conjunction with multiple-site optical recording techniques (cf. Grinvald et al., 1988). Several groups have used this approach to monitor evoked activity in olfactory bulbs of the tiger salamander, *Ambystoma tigrinum*. Most of this work has involved electrical stimulation of the olfactory nerve fibers (Orbach and Cohen, 1983; Kauer, 1988; Senseman et al., 1990; Cinelli and Salzberg, 1992), although dye signals also have been recorded in response to odor stimulation (Kauer et al., 1987; Cinelli and Kauer, 1992).

Two types of voltage-sensitive dye signals have been observed in the olfactory bulb after electrical stimulation of the olfactory nerve fibers: (1) an initial fast, "spike-like" depolarization in the olfactory nerve layer and (2) a secondary, slow depolarization within deeper layers. There is general agreement that the initial fast signal represents a presynaptic compound action potential in the primary olfactory receptor axons and that the slower depolarization reflects activity in the bulb's postsynaptic neurons (Orbach and Cohen, 1983; Senseman et al., 1990; Cinelli and Salzberg, 1992). There is less agreement, however, on which neuronal population is most directly responsible for the postsynaptic signal. Cinelli and Salzberg (1990, 1992) have argued that within the external plexiform layer, the slow depolarization largely reflects activity in mitral–tufted cell dendrites, whereas Wellis and Kauer (1993) argue that these signals largely reflect the activity in granule cell dendrites.

It should be possible to differentiate between signals generated by mitral–tufted cells and granule cells from a direct comparison of the signal waveforms recorded from the external plexiform and glomerular layers. The external plexiform layer contains the dendrites of both mitral–tufted cells and granule cells, but only the dendrites of mitral–tufted cells extend into the glomerular layer. If mitral–tufted cells are the primary source of the optical signals, signal waveforms should be similar across these two layers. Conversely, large differences in signal waveforms would suggest that additional cell types are involved. A direct comparison of signal waveforms is difficult in the salamander because the border between these layers is indistinct, even in slices (Cinelli and Salzberg, 1992). To address this problem, I used horizontal slices prepared from rat olfactory bulbs (Hajos et al., 1992; Nickell et al., 1994) in which the boundary between the glomerular and external plexiform layers is quite distinct. A broader aim was to provide additional insight into the flow of the afferent stream through the glomerular layer. Glomeruli are the most conspicuous feature of the vertebrate olfactory bulb (Shepherd, 1990; Farbman, 1992)

Received April 20, 1995; revised Sept. 25, 1995; accepted Sept. 25, 1995.

This work was supported by grants from the National Science Foundation (BNS-8507594), National Institutes of Health (GM 08194, 07717), the Texas Advanced Research Program (ARP 2222), the San Antonio Area Foundation, and Silicon Graphics. I thank Thomas Nickell for demonstrating the rat olfactory slice preparation, his participation in some early experiments, and many helpful discussions during the course of this work. Joel Solis is acknowledged for his excellent technical support and Barry Rhoades for his helpful discussions. I especially thank Larry Cohen for providing the data acquisition software and for his critical reading of an early draft of this manuscript.

Correspondence should be addressed to David M. Senseman at the above address.

and are believed to play a central role in odor quality discrimination (Le Gros Clark, 1951). Despite their presumed importance, the functional role of glomeruli has remained largely speculative (Scott et al., 1993).

A preliminary report of this work has appeared elsewhere in abstract form (Solis et al., 1993).

MATERIALS AND METHODS

Preparation. Experiments were performed on juvenile and adult Sprague–Dawley rats weighing 90–500 gm. Animals were placed under deep anesthesia with methoxyflurane (Metofane, Pitman–Moore) before decapitation in a small animal guillotine. Dorsal and lateral cranial surfaces were removed to expose the olfactory bulbs and cortex. During this procedure, ice-cold mammalian Ringer's solution was applied periodically to the exposed brain tissue to slow metabolic activity. A small, flexible spatula, fashioned from a thin sheet of mylar film, was used to sever the fine nerve fascicles passing through the cribriform plate. After the bulbs were freed from their afferent attachments, the entire brain was removed from the skull and immersed in chilled (4°C) mammalian Ringer's solution (125 mM NaCl, 5.0 mM KCl, 2.0 mM $MgSO_4$, 3.0 mM $CaCl_2$, 1.25 mM NaH_2PO_4, 25.5 mM $NaHCO_3$, and 10 mM D-glucose) for 1–3 min. The brain was then placed ventral side down on a piece of Parafilm and transected with a razor blade through the anterior cortex, roughly parallel to the rostral–ventral surface of the olfactory bulbs. The tissue block containing the bulbs and anterior cortex was then glued with cyanoacrylate adhesive to the stage of a vibratome ventral side up. The cut cortical surface rested directly on the stage, and the olfactory bulbs were supported by a small agar slab so that their longitudinal axes were roughly parallel to the plane of section. After the horizontal sections (400 μm thick) were cut, they were placed in shallow wells of an incubation chamber maintained at room temperature (18–24°C) and flushed with a continuous supply of 95% O_2/5% CO_2 for 30–60 min before staining.

Dye staining. After the recovery period, slices were stained for 60–90 min with the voltage-sensitive dye RH155 (Grinvald et al., 1982a), obtained from a commercial supplier (Nippon Kankoh-Shikiso Kenykyusho, Okayama, Japan). The minimum amount of dye solution (0.5 mg/ml normal Ringer's) needed to cover the slice surface was added to each well using a small Pasteur pipette. The dye stream was applied with sufficient force to dislodge the slice from the chamber bottom to ensure the dye's access to both slice surfaces. At the end of the staining period, excess dye was washed out with fresh saline and the slices were allowed to recover a minimum of 30 min before the first experimental trial.

Drugs and ionic manipulations. All drug solutions were prepared immediately before use and were tested by bath application. The competitive antagonist of GABA, bicuculline methiodide (BMI), was obtained from Research Biochemicals (Natick, MA). The noncompetitive GABA antagonist picrotoxin (PTX) and the Cl^- current inhibitor 4-acetamido-4′-isothiocyanatostilbene-2,2′-disulfonic acid (SITS) were obtained from Sigma (St. Louis, MO). Low-chloride Ringer's solution was prepared by equimolar replacement of NaCl with sodium propionate (Nowycky et al., 1981).

Electrical stimulation. A single stained slice was pinned to the bottom of a simple recording chamber containing two small plastic suction electrodes (50–100 μm inside tip diameter, 1.0–1.5 mm center-to-center tip separation). The slice was positioned so that the olfactory nerve layer pressed against the electrode tips. A slight suction was applied to draw some of the tissue into the electrode tip. Microstaples fashioned from fine tungsten wire (0.1 mm diameter) secured the slice and the suction electrodes to a slab of clear Sylgard resin attached to the chamber's glass bottom (see Fig. 1*A*). A four-channel, optically isolated electronic stimulator (Model 800, WP Instruments, New Haven, CT) delivered constant current pulses (1.5 mA, 0.5 msec duration) to the electrodes under computer control.

Optical recording and video imaging. The preparation was transilluminated with filtered light (720 ± 30 or 730 ± 40 nm) from a 100 W tungsten–halogen lamp driven by a stabilized DC power supply (Model 6264B, Hewlett-Packard Instruments, Rockville, MD). A 16× (0.5 NA) water immersion objective (Carl Zeiss, Oberkochen, Germany) projected a real image of the preparation onto a 464 element silicon photodiode array (Model MD-464, Centronic, Newbury Park, CA) mounted on the trinocular tube of a compound microscope (Model UEM, Carl Zeiss) (see Fig. 1*A*). With this objective, each photodiode element monitored activity in a 38 × 38 × 400 μm^3 tissue volume. The photocurrent generated by each diode element was separately amplified and filtered before being fed into a custom-designed 512 channel analog-to-digital converter and transferred to a 32 bit MC68030-based computer system (Model MVME-147, Motorola Microsystems Division). The DC signal component was removed by a passive AC filter with a 300 msec coupling time constant. High-frequency noise was reduced by an active, four-pole Bessel filter with a cutoff frequency of 2 kHz. Software used for data acquisition was provided by Dr. Larry Cohen (Yale Medical School). Further details about the amplification and digitization subsystems can be found elsewhere (Wu and Cohen, 1993). At the end of an experiment, the photodiode array assemble was replaced with a conventional video camera (Model C2400, Hamamatsu Photonics, Hamamatsu City, Japan), and a high-resolution image (512 × 512 pixels) of the preparation was acquired using a 4× microscope objective. The image was initially stored on an optical disk memory recorder (Model TQ-2025F, Panasonic, Secaucus, NJ) and later digitized with a commercially available image processor (Series 151, Imaging Technology, Woburn, MA).

Data display and analysis. Diode array and video data were combined and displayed on a 64 bit UNIX-based color graphics workstation (Iris Indigo XS24, Silicon Graphics, Mountain View, CA) using custom software (Senseman et al., 1990; Senseman and Rea, 1994). The software suite allowed optical signals to be analyzed quantitatively as analog waveforms or to be integrated with video image data to visualize directly the spatiotemporal spread of excitation. Statistical and graphical analyses were performed using Mathematica 2.0 (Wolfram Research, Champagne, IL) and ACE/gr (Center for Coastal and Land-Margin Research, Oregon Graduate Institute of Science and Technology, Beaverton, OR) on the SGI Indigo computer.

RESULTS

Laminar organization of signal waveforms

In previous optical studies of salamander and skate olfactory bulb slices, orthodromic stimulation evoked a fast, spike-like depolarization in the olfactory nerve layer and a large, but slower, depolarization within the external plexiform layer (Cinelli and Salzberg, 1990, 1992). A large depolarization with similar waveform properties also has been recorded in the external plexiform layer of turtle olfactory bulb slices (Senseman, 1994). In rat olfactory bulb slices, however, peak amplitudes of the external plexiform layer signals were small compared with olfactory nerve and glomerular layer signals. In only a few preparations were the external plexiform layer signals large enough to be observed clearly above the baseline noise (Fig. 1*B*).

In every preparation examined, transition from large to small amplitude signals occurred abruptly at the border between the glomerular and external plexiform layers. The sharpness of this transition can be seen in Figure 1*D*, which shows the analog waveforms recorded by each element in the 464 element array using a "page display" format. (In this format, the output from each detector is plotted relative to its location within the photodiode array.) Large-amplitude glomerular layer signals are replaced by low-amplitude external plexiform layer signals within one to two detectors corresponding to a linear distance of ~40–80 μm. From Figure 1*C* it can be seen that the transition occurs at the boundary between the glomerular and external plexiform layers.

Primary afferent depolarization and glomerular attenuation

Glomerular attenuation (Freeman, 1974a,b) is a prominent feature of orthodromic olfactory bulb activation in mammalian and nonmammalian vertebrate species. Pairs of electric shocks delivered to the olfactory nerve with interstimulus intervals ranging from 0.1 to 5 sec led to a significant reduction in the magnitude of a second "test" response. Depression of the test response has been observed electrophysiologically as (1) a depression of bulbar field potentials (Ottoson, 1959; Orrego, 1961; Nicoll, 1972; Freeman, 1974a,b; Jahr and Nicoll, 1981; Nowycky et al., 1981; Wal-

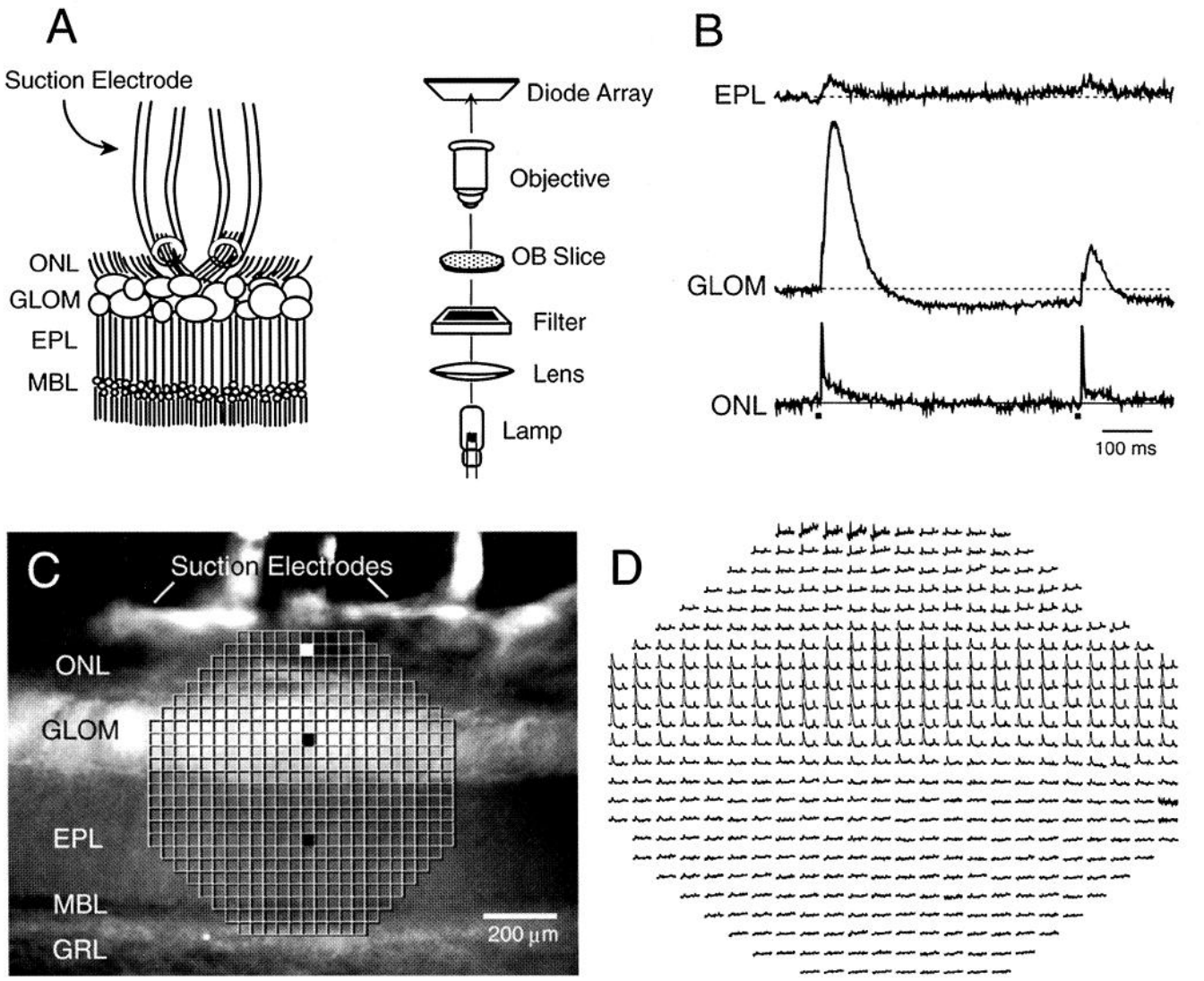

Figure 1. Experimental arrangement and representative voltage-sensitive dye signals. *A*, Semidiagrammatic representation of a rat olfactory bulb slice preparation is shown at *left*. For orthodromic stimulation, part of the olfactory nerve layer (*ONL*) was drawn into the tip(s) of one or two plastic suction electrodes (50–100 μm inside diameter). Tip separation for electrode pairs was 0.8–1.2 mm. Drawing at *right* shows optical arrangement for voltage-sensitive dye recording (see Materials and Methods). *B*, Three traces representative of the signal waveforms recorded from the olfactory nerve layer (*ONL*), the glomerular layer (*GLOM*), and the external plexiform layer (*EPL*). In this and in all other records, a decrease in light intensity is plotted upward. Peak amplitude of the glomerular layer signal represents a fractional change in light intensity of $\sim 2 \times 10^{-3}$. Records were obtained in a single experimental trial without signal averaging. Note the relatively small amplitude of the external plexiform layer response compared with the olfactory nerve layer and glomerular layer responses. *Small boxes* below the x-axis indicate the onset of the initial "conditioning" pulse and the subsequent "test" pulse. *C*, Outline of the 464 element photodiode array is shown superimposed on a photomicrograph of the preparation. The *three filled diode elements* in the grid indicate the recording locations for the three traces shown in *B*. The pair of suction electrodes used for olfactory nerve layer stimulation are visible at the *top* of the image. *MBL*, mitral body layer; *GRL*, granule cell layer. *D*, Page display showing the complete data set recorded in a single trial. Optical signals have been plotted in a two-dimensional array corresponding to the signal's origin within the 464 element silicon photodiode array. Spatial differences in illumination intensity have been corrected by dividing the signal from each detector element by the detector's DC light level. Optical noise can be observed in some traces near the edge of the detector. Total duration of each trace is 750 msec.

drow et al., 1981), (2) a reduction in single-unit activity (Getchell and Shepherd, 1975a,b; Waldrow et al., 1981), (3) a suppression of summed, synaptically evoked potentials in mitral and granule cells (Mori et al., 1981; Hamilton and Kauer, 1988; Wellis and Scott, 1990), and (4) a decrease in the amplitude of voltage-sensitive dye signals (Orbach and Cohen, 1983; Cinelli and Salzberg, 1990, 1992). Clear evidence of glomerular attenuation also was observed in the voltage-sensitive dye signals recorded from the glomerular layer of rat olfactory bulb slices. Peak amplitude of the test response was reduced by 66 ± 6% (mean ± SD, $n = 32$) when the test stimulus was preceded 500 msec earlier by a conditioning stimulus of similar amplitude and duration.

Primary afferent depolarization has been proposed as the causal mechanism underlying glomerular attenuation in frog olfactory bulbs. Jahr and Nicoll (1981) found that a single electrical shock depolarized the frog's olfactory nerve for as long as 1 min with a half-decay time of ~10 sec as measured from the cut end of the transected nerve using the sucrose gap technique. This depolarization was not recorded in isolated nerves but only in nerves attached to the bulb. They also observed that the time course of

the olfactory nerve depolarization correlated closely with a reduction in the efficacy of the orthodromic stimulation to drive secondary bulbar neurons. Based on these data, Jahr and Nicoll (1981) suggested that nerve stimulation produced a sustained depolarization of the olfactory nerve terminals that led to a reduction of transmitter release from the presynaptic terminals and, by extension, the development of paired-pulse depression.

I examined the voltage-sensitive dye signals within the olfactory nerve layer to find evidence that might support Jahr and Nicoll's hypothesis. Because these investigators had been able to record the passive spread of primary afferent depolarization from the end of the olfactory nerve (a relatively long distance from the site of depolarization), I expected the depolarization to be clearly visible within the nerve layer, where the axonal fibers are much closer to their terminal synapses. No evidence was found, however, that electrical stimulation of the nerve layer generated a sustained depolarization of the afferent fibers. Brief electrical stimulation, sufficient to elicit pronounced glomerular attenuation, evoked only a fast, transient depolarization in the olfactory nerve layer that returned to baseline levels well before the onset of the test pulse (e.g., Fig. 1*B*). A small but consistent reduction was generally observed in the peak amplitude of the compound action potential evoked by the test pulse. In the experiment shown in Figure 1*D*, peak amplitude of the compound action recorded by each element was reduced by 5 ± 0.5% (mean ± SD, $n = 31$). It seems unlikely, however, that a 5% decrease in the peak amplitude of the presynaptic signal can account fully for a >60% reduction in the postsynaptic response.

Intrinsic glomerular layer signal and the "late hyperpolarization"

In salamander olfactory bulb slices, the slow depolarization recorded in the external plexiform layer is followed by a period in which the optical signals fall below the initial baseline level for a sustained period (>300 msec). This component of the optical response has been called the "late hyperpolarization" and is presumed to reflect granule cell inhibition of the mitral–tufted cell dendrites (Cinelli and Salzberg, 1992). Similar periods of inhibition also have been reported in the optical signals recorded from the external plexiform layer in salamander olfactory bulbs after odor stimulation of the olfactory mucosa (Kauer et al., 1987).

In the current series of experiments, glomerular layer depolarizations also were followed by a period in which the optical signal dropped below the baseline (e.g., Fig. 1*B*), and it was initially assumed that this component was equivalent to the late hyperpolarization observed previously in the salamander. Control experiments revealed, however, that this negative baseline shift was attributable, at least in part, to an intrinsic optical response (Grinvald et al., 1982b; Konnerth et al., 1987). Optical recordings taken from slices before staining revealed a slow increase in light transmission through the glomerular layer after nerve layer stimulation. The increased transmission commenced within 10 msec of stimulation, reached a peak between 150 and 250 msec poststimulation, and declined slowly over the next 1000 msec. As would be expected of an intrinsic signal, neither the amplitude nor the waveform of this response was affected by changes in illumination wavelength between 540 and 850 nm (data not shown). Intrinsic optical signals were not observed within the olfactory nerve or external plexiform layers.

To determine how the intrinsic signal distorted the extrinsic, dye-related optical signal, I compared glomerular layer signals from stained slices that were illuminated with light passed through a "narrow" interference filter (720 ± 30 nm) with signals recorded using a "broad" interference filter (730 ± 40 nm). The broad filter would be expected to increase the amplitude of the intrinsic component to a greater extent than the extrinsic component because the additional light passed by the broad filter would be composed of wavelengths farther from the peak of the dye's activity spectrum. As can be seen in Figure 2*C*, the broad filter slightly increased the peak amplitude of the glomerular layer depolarization but greatly exaggerated the magnitude of the late hyperpolarization. The most straightforward interpretation of this result is that the optical signal recorded in the glomerular layer is composed of both extrinsic and intrinsic signal components. Because the intrinsic signal component develops slowly, its distortion of the initial depolarization is comparatively minor. By 100–200 msec poststimulation, the magnitude of the intrinsic signal is sufficiently large that it forces the optical signal below baseline level, generating what appears to be a late hyperpolarization.

Whether the intrinsic optical signal masks a true membrane hyperpolarization in rat olfactory bulb slices is difficult to assess. Subtraction of a "reference signal" recorded at a wavelength outside the dye's activity spectrum (e.g., 810 nm) has been used previously to reduce distortion in voltage-sensitive dye signals recorded from hippocampal slices (Grinvald et al., 1982b). Initial attempts to apply a similar correction procedure to rat olfactory bulb slices were only partly successful. Relatively small differences in the scaling factor used to adjust the magnitude of the reference signal (see Grinvald et al., 1982b) led to glomerular layer depolarizations followed by a period of low-level "hyperpolarization," no "polarization," or even by low levels of "depolarization." Given the uncertainty of this correction procedure, no attempt was made to remove or otherwise reduce the intrinsic component of the optical signal. Consequently, no particular significance was attributed to slow shifts in the signal baseline ("DC level"). Analysis of glomerular layer signal waveforms was restricted to their onset, initial rate-of-rise, peak amplitude and their time-to-peak because these "fast" components did not appear to be significantly distorted by the slower, intrinsic changes in tissue opacity that invariably followed nerve stimulation.

Initial transformation of the olfactory processing stream

With relatively fast recording speeds (<0.2 msec/frame), it was possible to observe directly the olfactory receptor volley propagate through the olfactory nerve layer and into the glomerular layer (Fig. 3*B*). Within the nerve layer, the amplitude of compound action potential remained fairly constant but declined as it entered the glomerular layer. The decline was sufficiently rapid that the presynaptic signal dropped into the baseline noise as it approached the external plexiform layer (Fig. 3*D*). It is presumed that the fall in signal amplitude mirrors the spatial distribution of presynaptic fibers within the glomerular layer. As the afferent stream moves proximally through the layer, the number of olfactory receptor axons remaining in the stream would be expected to decline as individual olfactory receptors leave to establish their terminal synaptic contacts with mitral and periglomerular cells. The fact that the presynaptic signal did not cross into the external plexiform layer is consistent with the histological evidence that all olfactory receptor axons terminate within the glomerular layer, at least in adult rats (Shepherd, 1990).

Mammalian olfactory receptor axons do not branch before they reach the glomerular layer, but they do ramify within a

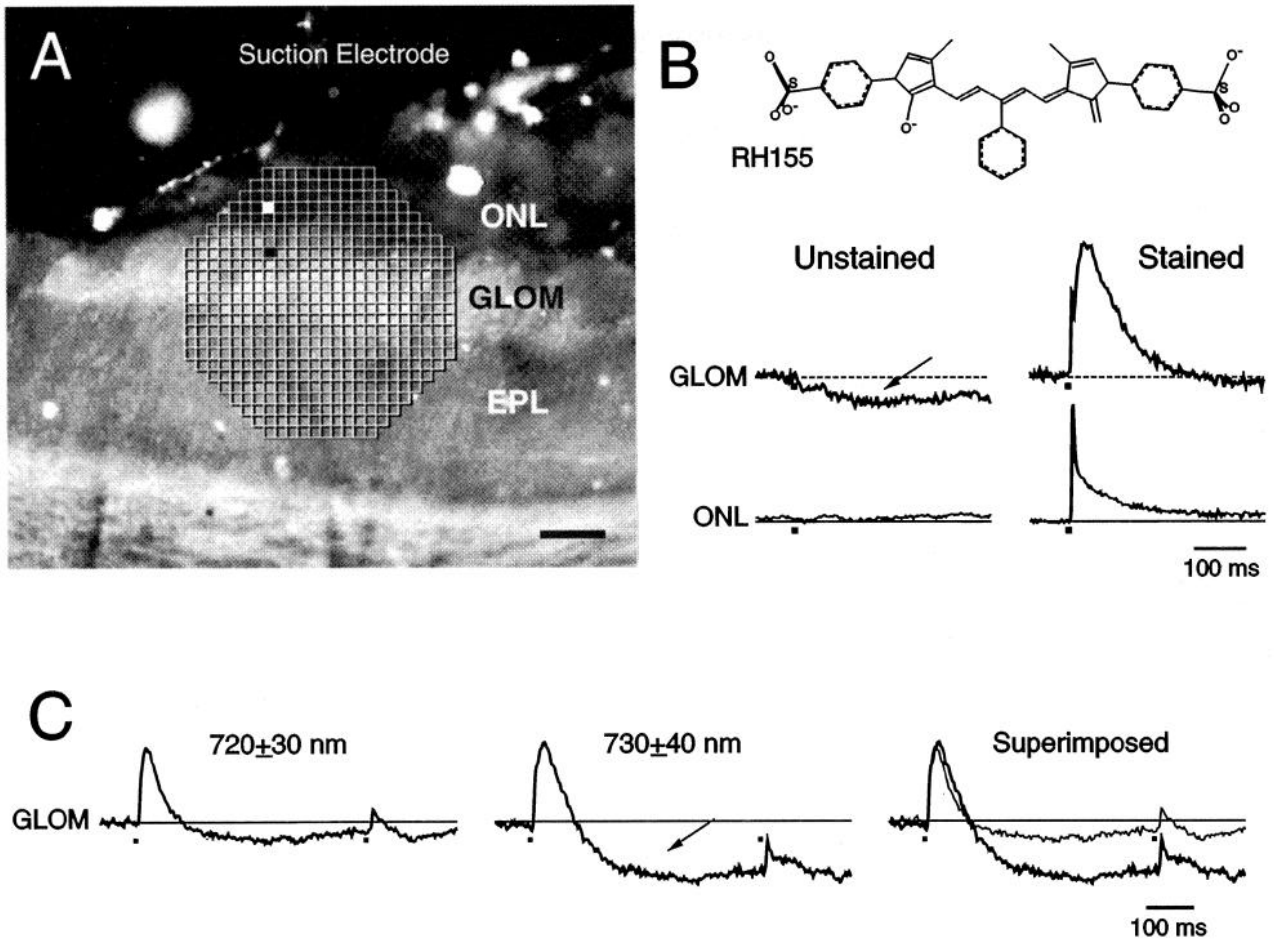

Figure 2. Intrinsic and extrinsic optical signals evoked by olfactory nerve stimulation. *A*, Outline of photodiode array shown superimposed on a photomicrograph of the slice preparation. *Filled grid boxes* indicate recording locations for the olfactory nerve layer (*ONL, white*) and glomerular layer (*GLOM, black*) signals shown in *B*. In this photomicrograph, the outline of the suction electrode at the top of the image is indistinct. Scale bar, 200 μm. *B*, Comparison of signals recorded before and after staining. *Traces* at *left* were recorded from an unstained slice and show a relatively large intrinsic signal in the glomerular layer (*arrow*) after olfactory nerve stimulation. *Traces* at *right* were recorded from the same slice after staining with a 0.5 mg/ml solution of the dye RH155 for 60 min. Signal amplitude of the pair of traces shown on the *left* has been reduced by 2× to account for the 2× higher level of light transmission through the unstained slice. Chemical structure of the voltage-sensitive dye RH155 is shown above the traces. *C*, Relative contribution of the intrinsic signal to the extrinsic, dye-related optical signal recorded in the glomerular layer. *Trace* at *left* was recorded using a "narrow" interference filter (720 ± 30 nm), whereas the *middle trace* shows the signal recorded by the same detectors using a "broad" interference filter (730 ± 40 nm). A superposition of these two records is shown at the *right* with the *thicker line* representing the *trace* recorded with the "broad" filter. Note that the broad filter increases selectively the downward ("hyperpolarizing") component of the optical response but not the initial upward (depolarizing) component. *Traces* shown in *C* were obtained from a similar, but different, preparation from the one shown in *A*. *Small boxes* below x-axes indicate onset of conditioning and test pulses to the olfactory nerve layer.

single glomerulus as they form their terminal connections. Moreover, their synaptic terminals are relatively large compared with the thin, unmyelinated axons from which they arise (Shepherd, 1990). This sudden increase in membrane surface area might be expected to slow the conduction velocity within the glomerular layer. Spatial inhomogeneities in conduction velocities have been observed, for example, in unmyelinated vagal afferents (Duclaux et al., 1976). To examine whether the conduction velocity changed as the axons enter the glomerular layer, I plotted the distance traveled by the compound action potential as a function of its time-to-peak (Fig. 3*C*). No evidence of a break-point was found to indicate a change in velocity; the relationship between distanced traveled and time-to-peak was well fitted with a straight line ($r^2 = 0.99$, $n = 10$). The slope of the least-squares fit gave a conduction velocity of 0.25 (±0.01) m/sec, which is somewhat below the range of 0.3–0.5 m/sec for mammalian species cited by Shepherd (1979), but not unreasonable considering the lower temperature (~20°C) at which these optical measurements were made.

The reciprocal relationship between pre- and postsynaptic responses in the glomerular layer also can be seen in Figure 3*D*. As the presynaptic compound action potential crosses into the glomerular layer and begins to decline, the postsynaptic depolarization appears out of the baseline noise and increases rapidly in amplitude. The postsynaptic signal continues to increase in size until about midway through the glomerular layer, where it reaches a maximum and then declines steadily, losing ~10% of its peak amplitude for every 25 μm of proximal travel. By the time the response reaches the external plexiform layer, its amplitude has been reduced by more than an order of magnitude.

Interactions between overlapping afferent streams

The results presented in Figure 4 are representative of several experiments ($n = 12$) in which two overlapping afferent streams

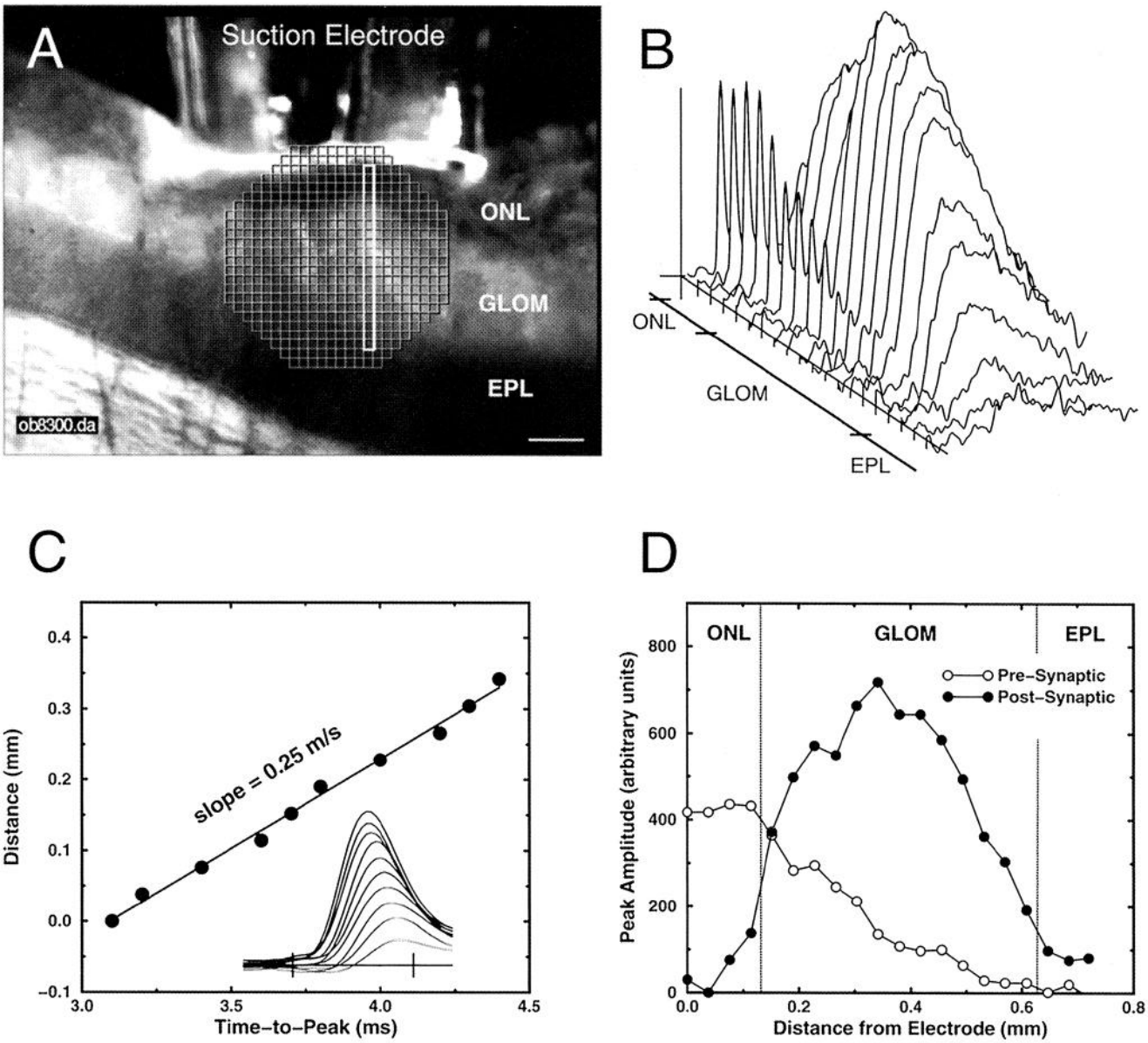

Figure 3. Propagation of the presynaptic signal and the development of the postsynaptic response. *A*, Outline of the photodiode array is shown superimposed on a photomicrograph of the preparation. The column of diode elements outlined in *white* provided the waveform data shown in *B*. The suction electrode used for electrical stimulation of the olfactory nerve layer (*ONL*) can be observed at the *top* of the image. Scale bar, 200 μm. *B*, Optical signal waveforms recorded at 0.169 msec/frame represent the average of four trials (20 sec intertrial interval). A staggered format has been used to give a three-dimensional view of the response across the different bulbar layers. Total duration of each trace is 75 msec. *C*, Graphical analysis of the conduction velocity of the presynaptic signal presented in *B*. *Inset* shows a superimposed and expanded display of the traces presented in *B* that were used to generate the curve. The first tic mark on the x-axis indicates the onset of stimulation, and the distance between the first and second tic marks indicates 5 msec. *D*, Graph showing peak amplitudes of the presynaptic responses (*open circles*) and postsynaptic responses (*closed circles*) plotted as a function of distance from the stimulating electrode.

→

Figure 4. Radiation of the glomerular layer signals from the stimulation epicenter. *A*, Outline of the photodiode array is shown superimposed on a photomicrograph of the preparation. The row of diode elements outlined in *black* provided the waveform data shown in *B*. The two suction electrodes, labeled *L* and *R*, visible at the top of the image were used to stimulate the olfactory nerve layer (*ONL*) with 1.0 mA, 0.5 msec pulses. Scale bar, 200 μm. *B*, Optical signal waveforms recorded in response to a pair of pulses (500 msec separation) delivered by the *R* electrode (*Ba*), by the *L* electrode (*Bb*), or conjointly by both electrodes (*Bc*). Signals were recorded in a single trial and have been staggered to give a 3-dimensional view of the response between the two electrodes. *Double-headed arrow* in *Bc* indicates orientation of traces with respect to the image in *A*. *Single-headed arrow* in *Ba* shows an unusually large response (hot spot). The pair of *lines* below each set of traces indicates stimulus onset and provides a 500 msec time calibration between the two tic marks. *C*, Graph showing peak amplitudes of conditioning responses shown in *Ba* (*R*-stimulated, *open circles*) and *Bb* (*L*-stimulated, *filled circles*) as a function of distance from the *L* electrode. *Arrow* indicates data point corresponding to the hot spot indicated in *Ba*. *D*, Graph comparing peak amplitudes of conditioning responses observed with conjoint electrode stimulation (*filled boxes*) with the peak responses predicted by the algebraic summation of the two curves presented in *C* (*open boxes*). *Arrow* indicates data point corresponding to the hot spot indicated in *Ba*. *E*, Graph showing the peak amplitude of the response as a function of distance from the stimulus epicenter. *Solid line* shows a normal distribution probability curve with an SD (σ) of 410 μm.

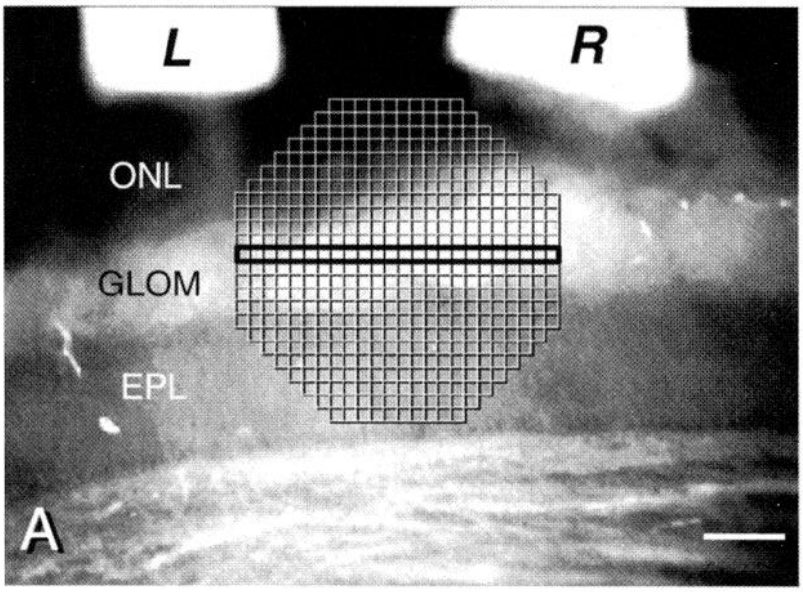
L
R
ONL
GLOM
EPL
A

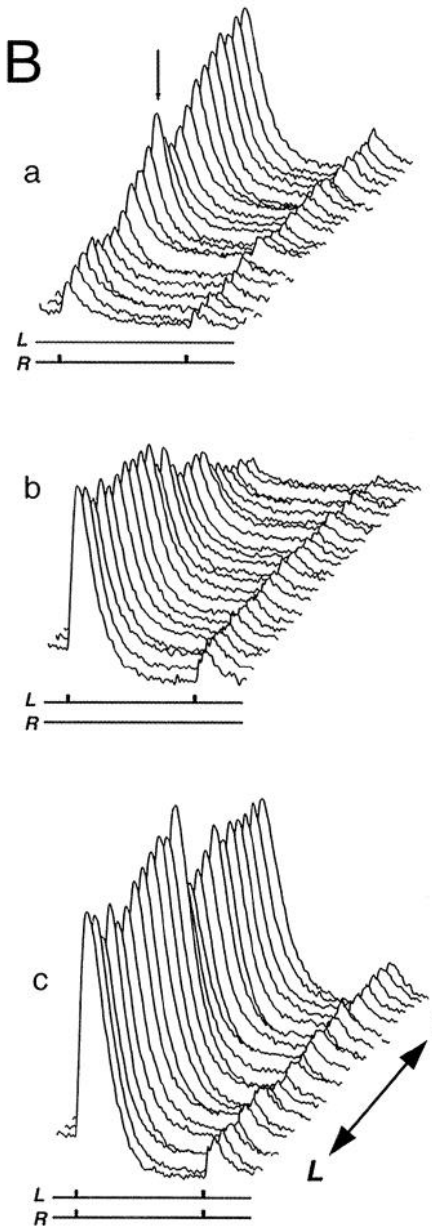
B
a
L
R
b
L
R
c
R
L
L
R

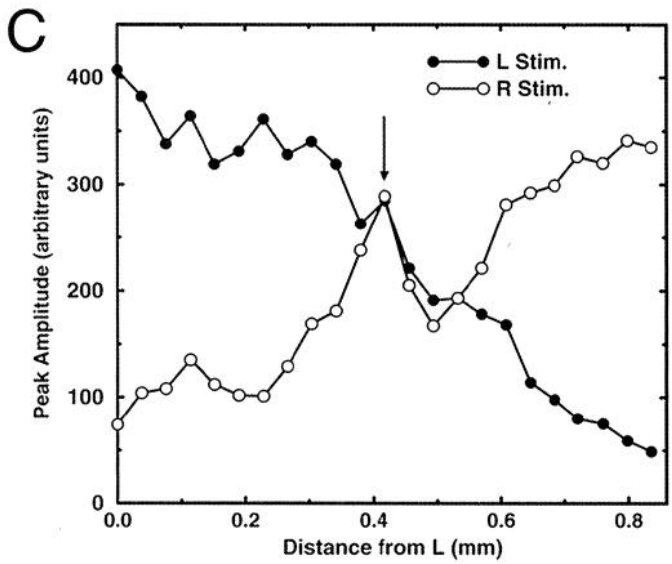
C
L Stim.
R Stim.
Peak Amplitude (arbitrary units)
0
100
200
300
400
0.0
0.2
0.4
0.6
0.8
Distance from L (mm)

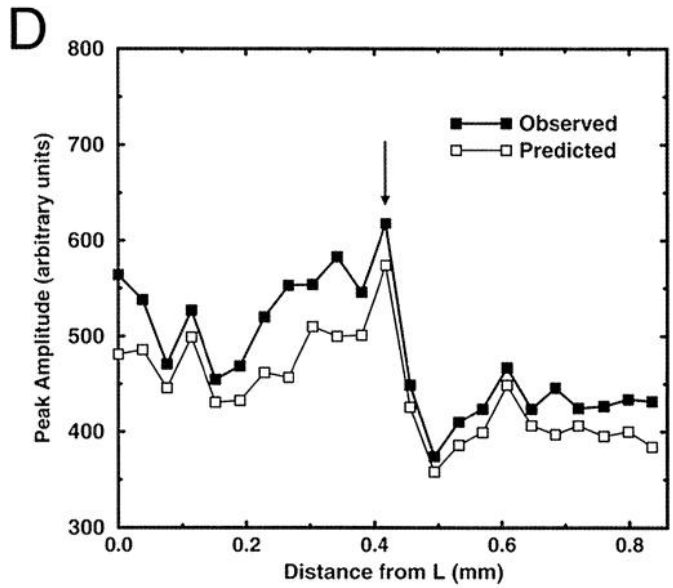
D
Observed
Predicted
Peak Amplitude (arbitrary units)
300
400
500
600
700
800
0.0
0.2
0.4
0.6
0.8
Distance from L (mm)

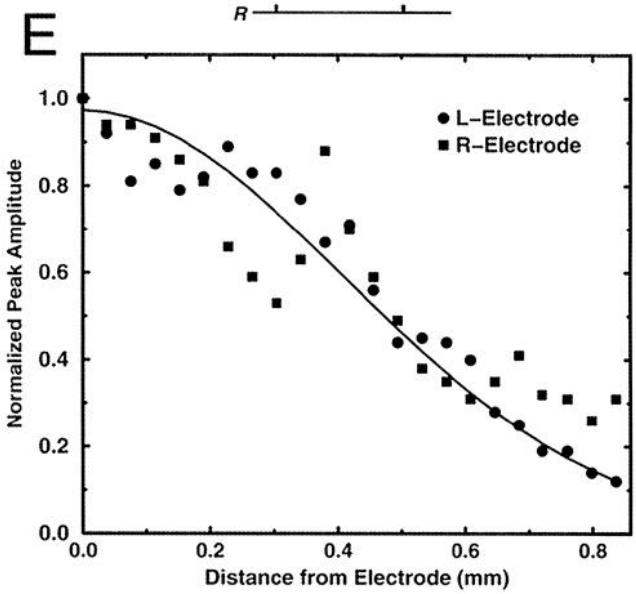
E
L–Electrode
R–Electrode
Normalized Peak Amplitude
0.0
0.2
0.4
0.6
0.8
1.0
0.0
0.2
0.4
0.6
0.8
Distance from Electrode (mm)

were generated using a pair of suction electrodes (left, *L*; right, *R*) with a tip separation of ~1.0 mm. These experiments revealed that the flow of afferent streams through the glomerular layer was governed by four general principles. First, evoked responses were not sharply focused into a narrow, "on-beam" afferent stream, but radiated from the stimulation epicenter (Fig. 4*B,C*). Second, as the stream flowed into some regions of the glomerular layer, anomalously large excitatory responses ("hot spots") were sometimes observed. The presence and location of a hot spot within the glomerular layer did not vary, but remained stable from trial to trial (*arrow*, Fig. 4*B–D*). Hot spots did not result from uneven field illumination because they were not eliminated by "on-off" normalization (see Senseman and Rea, 1994). In some, but not all, experiments, hot spots could be seen to correspond to unusually large glomeruli. Third, in regions where two afferent streams overlapped in space and time, peak amplitudes of the glomerular response summated (Fig. 4*D*). Summated responses evoked by conjoint electrical stimulation (*solid boxes*) could be predicted by simple addition of the individual responses evoked by a single electrode (*open boxes*). Heterosynaptic facilitation, if present, was minor. Fourth, the intensity of the glomerular layer signal declined from the stimulus epicenter according to a normal distribution with an SD (σ) of 410 μm (Fig. 4*E*). Within this context, it is interesting to note that Freeman (1974b) also found that a normal distribution with an SD (σ) of 410 μm characterized the spatial decline in responsiveness of presumptive periglomerular cells from the stimulus epicenter in cat and rabbit olfactory bulbs.

Overlapping processing streams and glomerular attenuation

Although glomerular attenuation generally is studied with the same electrode delivering both the conditioning and the test stimuli (Waldrow et al., 1981; Cinelli and Salzberg, 1992), it is not necessary for the conditioning and test inputs to reach the glomerular layer via the same afferent fibers. Freeman (1974a) found that significant glomerular attenuation could be generated in the cat olfactory bulb *in vivo* when separate electrodes were used to deliver the conditioning and test stimuli, provided that the interelectrode spacing was ≤1.5 mm. This also was true in rat olfactory bulb slices *in vitro*. Flow in one afferent stream attenuated the subsequent flow of another overlapping afferent stream. Figure 5*Ba* shows conditioning responses elicited by the *R* electrode and test responses elicited 500 msec later by the *L* electrode, and Figure 5*Bb* shows the results obtained in the reciprocal experiment. Peak amplitudes of the conditioning response evoked by the *R* electrode (*closed squares*) and *L* electrode (*open squares*) are shown in Figure 5*C*, along with the peak amplitudes of the test responses evoked by the *R* electrode (*closed circles*) and *L* electrode (*open circles*). At all points between the two electrodes, the peak amplitude of the test response (*circles*) is attenuated compared with the conditioning response (*squares*).

The magnitude of attenuation was found to be directly related to the magnitude of depolarization produced by the conditioning stream (Fig. 5*D*). Linear regression analysis of the data shown in Figure 5*D* gave the following results: $r^2 = 0.96$, slope = 0.60 ± 0.02 (±SD), y-intercept = −0.04 ($n = 46$). This means that 500 msec after the initial stream had passed through a localized region of the glomerular layer, the excitatory effects of a second afferent stream, arriving over a different population of olfactory nerve fibers, was reduced by a value equal to 60% of the peak depolarization generated by the preceding stream. It is somewhat surprising that the magnitude of depression appears to be completely independent of the magnitude of the stream arriving 500 msec later. Whether this second stream is quite large or quite small, it will be reduced by a percentage determined only by the magnitude of the earlier stream. It should also be noted that this percent reduction (i.e., the slope of the regression line) obviously will change as a function of the time interval between the arrival of the two streams, approaching zero as the time interval grows sufficiently large. A quantitative analysis of the temporal dependence of the slope parameter was beyond the scope of the current series of experiments.

Cl^- dependence of the glomerular layer response

Nowycky et al. (1981) found that in the presence of low-chloride solutions, orthodromic activation of mitral cells in the isolated turtle olfactory bulb was significantly enhanced. The prominent IPSP normally observed in mitral cells after olfactory nerve stimulation was replaced by a long-lasting excitatory potential that gave rise to several impulse discharges. When NaCl in the bathing media was replaced with sodium propionate in the current experimental series, the compound action potential recorded optically in the olfactory nerve layer was largely unaffected, whereas the peak amplitude of the conditioning response recorded in the glomerular layer almost doubled after a 25 min exposure (Fig. 6). Low $[Cl^-]_o$ also increased the peak amplitudes of conditioning responses recorded within the external plexiform layer, but to a lesser extent. Despite the large increase in the conditioning response, test responses recorded in either the glomerular layer or the external plexiform layer were largely unaffected after 25 min exposure to low-chloride Ringer's solution.

Nowycky et al. (1981) found that during prolonged exposure to low-chloride media (>30 min), mitral cells in the turtle olfactory bulb became depolarized and their baseline firing increased until normal chloride levels were re-established. Degenerative changes in rat olfactory bulb slices also were observed during prolonged exposure to low-chloride Ringer's solution (Fig. 6*C*), although little or no recovery was obtained after washing with normal Ringer's solution. The progressive loss of voltage-sensitive dye signals in low-chloride Ringer's solution was noteworthy in two respects. First, low-chloride-induced dysfunction was expressed primarily by second-order and possibly third-order neurons in the bulbar circuitry. After 35 min exposure, relatively robust activity could still be recorded optically from the presynaptic axons of the primary olfactory receptors, whereas evidence of evoked activity in the glomerular and external plexiform layers was largely eliminated. Second, loss of postsynaptic signals in the glomerular and external plexiform layers occurred at different times. After 30 min exposure to low-chloride Ringer's solution, the peak amplitude of the conditioning response recorded in the glomerular layer still exceeds the control value, whereas the conditioning response recorded in the external plexiform layer is essentially abolished.

Nowycky et al. (1981) suggested that because bath application of BMI, a competitive $GABA_A$ receptor antagonist, largely mimicked the excitatory effects of low-chloride media, the increased excitability of mitral cells after olfactory nerve stimulation could be explained simply by the removal of Cl^--mediated IPSPs. This hypothesis does not seem to explain the large increase in the glomerular layer response observed in rat olfactory bulb slices exposed to low $[Cl^-]_o$. In five experiments,

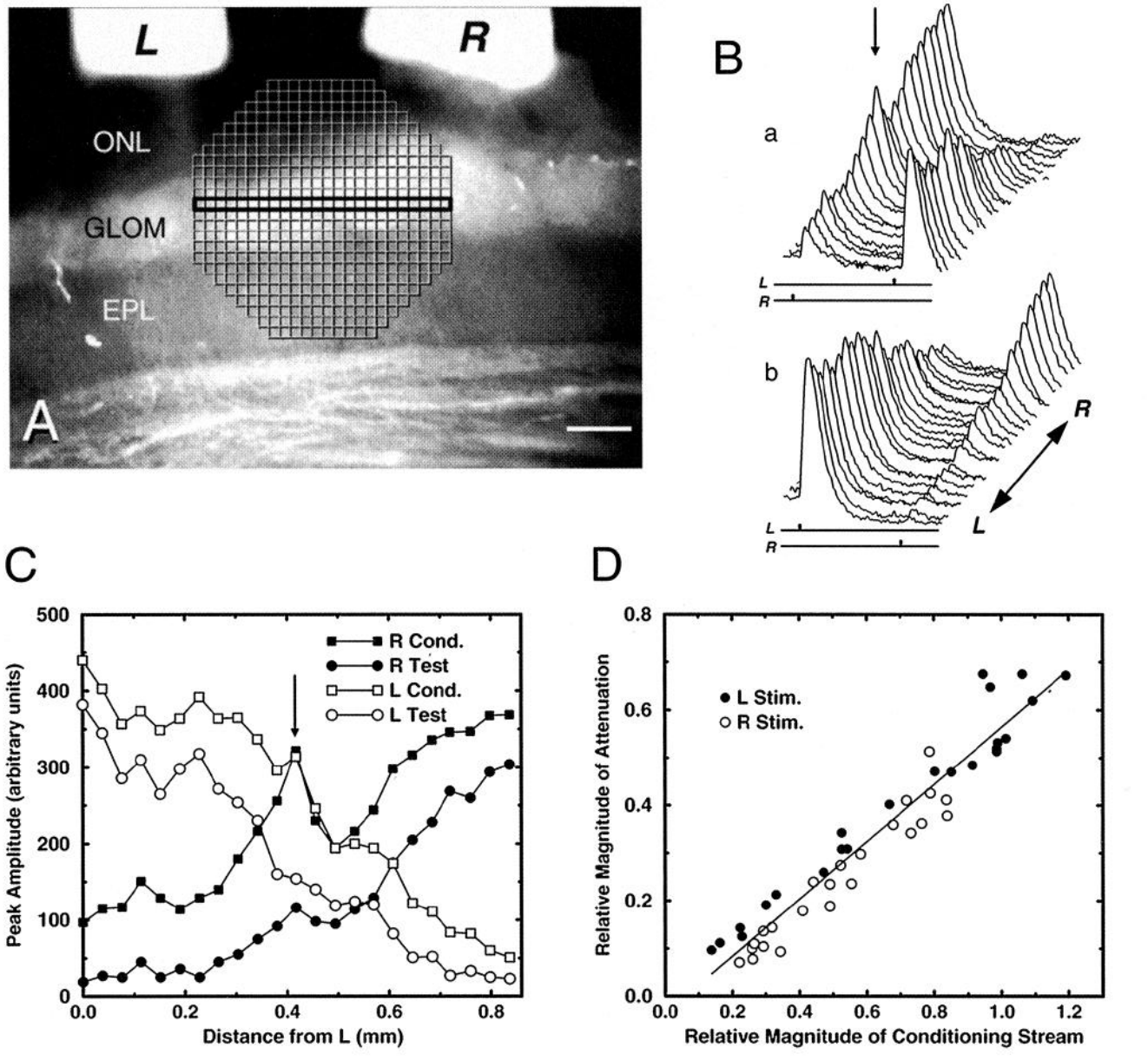

Figure 5. Glomerular attenuation produced by overlapping afferent streams. *A*, Outline of the photodiode array is shown superimposed on a photomicrograph of the preparation. This is the same slice preparation used in Figure 4. The row of diode elements outlined in *black* provided the waveform data shown in *B*. The two suction electrodes, labeled *L* and *R*, visible at the top of the image, were used to stimulate the olfactory nerve layer (*ONL*) with 1.0 mA, 0.5 msec pulses. Scale bar, 200 μm. *B*, Signal waveforms were recorded in a single trial in response to contralateral stimulation with the *R* electrode delivering the conditioning pulse and the *L* electrode delivering the test pulse (*Ba*), or the *L* electrode delivering the conditioning pulse and the *R* electrode delivering the test pulse (*Bb*). Interpulse interval was 500 msec. *Double-headed arrow* in *Bb* indicates orientation of traces with respect to the image in *A*. *Single-headed arrow* in *Ba* shows an unusually large response (hot spot). The pair of *lines* below each set of traces indicates stimulus onset and provides a 500 msec time calibration between the two tic marks. *C*, Peak amplitudes of conditioning responses (*boxes*) and test responses (*circles*) shown in *Ba* and *Bb* are plotted as a function of distance from the *L* electrode. *Open symbols* represent responses evoked by the *L* electrode; *filled symbols* represent responses evoked by the *R* electrode. *Arrow* indicates data point corresponding to the hot spot indicated in *Ba*. *D*, Graph illustrating the linear relationship between the relative magnitude of glomerular attenuation and the relative magnitude of a preceding conditioning stream. For each detector element surveyed, the relative magnitude of depression was defined as the difference in peak amplitude recorded in the absence and presence of a preceding conditioning stream generated by the other electrode 500 msec earlier. The difference between the two peak amplitudes was normalized by dividing the remainder by the sum of their two responses. The relative magnitude of the conditioning stream was simply the peak response evoked by the second electrode. This value was expressed relative to the largest response evoked by that electrode in the same trial.

bath application of PTX, a noncompetitive antagonist of $GABA_A$ receptors, or of BMI either singly or in combination had relatively little effect on the amplitude or the duration of the conditioning and test responses recorded in the glomerular layer (Fig. 6*D*). However, the peak amplitude of the conditioning response in the glomerular layer could be reduced significantly (>30%) with bath application of 1 mM SITS, a stilbene derivative that inhibits Cl^- current and conductances in a number of preparations (Knauf and Rothstein, 1971; Inoue, 1985; Gray and Ritchie, 1986; Dubin and Dionne, 1994) (Fig. 6*E*). The inhibitory effects of SITS could be partially reversed by washing in normal Ringer's solution.

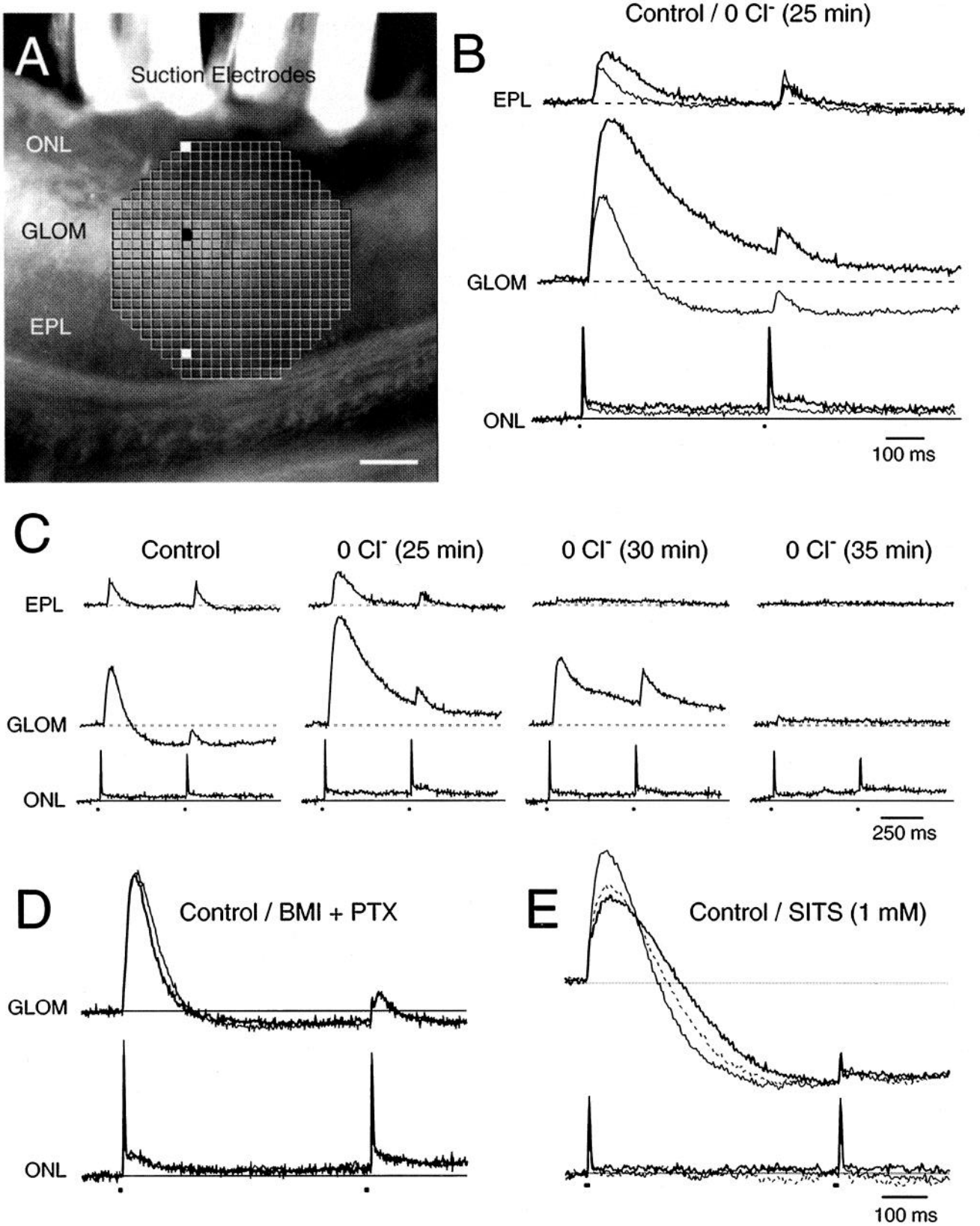
A
Suction Electrodes
ONL
GLOM
EPL
B
Control / 0 Cl⁻ (25 min)
EPL
GLOM
ONL
100 ms
C
Control
0 Cl⁻ (25 min)
0 Cl⁻ (30 min)
0 Cl⁻ (35 min)
EPL
GLOM
ONL
250 ms
D
Control / BMI + PTX
GLOM
ONL
E
Control / SITS (1 mM)
100 ms

DISCUSSION

Cellular basis of the glomerular layer optical signal

The present study provides the first evidence that the glomerular and external plexiform layers generate significantly different voltage-sensitive signals. Two lines of evidence suggest that the postsynaptic glomerular layer signal is largely dominated by evoked activity in periglomerular cells. Based simply on anatomical considerations, voltage-sensitive dye signals are much more likely to reflect activity in periglomerular cells than mitral–tufted cells. The relatively large size of mitral–tufted cells makes them good targets for microelectrodes but not particularly good sources for the generation of voltage-sensitive signals. In general, the amplitude of a voltage-sensitive signal will be directly proportional to the total surface area of stained membrane within the tissue volume monitored by an individual light detector element. Within a given tissue volume, a population of small cells will contribute more membrane area and thus generate a larger signal than a few large cells. Moreover, the population of mitral cells within the olfactory bulb is relatively low. In the rabbit, it has been estimated that periglomerular cells outnumber mitral cells 20:1, granule cells 200:1, and primary olfactory receptors 1000:1 (Allison and Warwick, 1949).

The fact that the optically recorded postsynaptic responses were largely confined to the glomerular layer (e.g., Figs. 1*B*, 3*C*) is also consistent with periglomerular cells being the primary source of the voltage-sensitive dye signals. In rats the cell bodies, dendrites, and axons of periglomerular cells are restricted to the glomerular layer (Pinching and Powell, 1971a,b,c). One would expect voltage-sensitive dye signals generated by these neurons to be confined to this layer. On the other hand, mitral–tufted cells support extensive dendritic trees within the external plexiform layer in addition to a synaptic tuft within the glomerular layer (Orona et al., 1984). Membrane potential changes generated in the synaptic tuft would be expected to spread readily, with little attenuation, into their dendritic trees (Rall and Shepherd, 1968; Shepherd, 1990). One would expect voltage-sensitive signals generated by mitral–tufted cells to be visible within the external plexiform layer as well as in the glomerular layer. Although the dendrites of mitral–tufted cells undoubtedly make some contribution to the overall voltage-sensitive dye signal, the small size of this signal within the external plexiform layer suggests that the magnitude of this contribution is relatively minor.

In addition to periglomerular cells, other cell types within the glomerular layer also would be expected to contribute to the overall glomerular layer signal in rough proportion to their population densities. Superficial short axon cells are the only other cell type that might occur in sufficient numbers to make a substantial contribution. In rats, superficial short axon cells have been reported to be relatively rare compared with periglomerular cells (Pinching and Powell, 1971a,b,c). On the other hand, more recent work in hamsters found superficial short axon cells to be almost as common as periglomerular cells (Schneider and Macrides, 1978). Furthermore, Schneider and Macrides (1978) have suggested that the rarity of superficial short axon cells in the rat is simply an artifact of fixation. However, until there is direct evidence to the contrary, it will be assumed that, in the rat, short axon cells are substantially less numerous than periglomerular cells and, therefore, that any contribution they make to the glomerular layer signal is relatively minor.

Cl^- efflux and periglomerular cell depolarization

Synaptically activated glomerular layer depolarization proved insensitive to bath application of the $GABA_A$ Cl^- channel blockers BMI and PTX, but could be decreased by the Cl^- channel blocker SITS and increased, at least in the short-term, by lowering $[Cl^-]_o$ (Fig. 6). One way to explain these findings is to assume that afferent input activates a SITS-sensitive Cl^- conductance in rat periglomerular cells and that $[Cl^-]_i$ is sufficiently high in these cells that the equilibrium potential for Cl^- (E_{Cl}) is above the normal resting membrane potential. Under these conditions, activation of this Cl^- conductance would lead to Cl^- efflux and membrane depolarization with normal $[Cl^-]_o$ and increased Cl^- efflux and increased depolarization in reduced $[Cl^-]_o$.

Some additional support for this idea comes from histological evidence showing that dendritic $[Cl^-]_i$ is unusually high in some rat periglomerular cells, suggesting that E_{Cl} is above the resting membrane potential (Siklos et al., 1995). Also, a slowly inactivating, voltage-sensitive Cl^- conductance has been identified recently in mudpuppy primary olfactory receptor neurons that can be blocked by a stilbene derivative related to SITS (Dubin and Dionne, 1994). In these receptors, E_{Cl} also appears to be above the resting membrane potential so that activation of this conductance is thought to produce sustained Cl^- efflux and a sufficient level of membrane depolarization to generate a burst of action of potentials (Dubin and Dionne, 1994). A slowly inactivating Cl^- conductance in rat periglomerular cells, therefore, could explain, at least in part, the sustained depolarization recorded optically in the glomerular layer after olfactory nerve layer stimulation.

In summary, fast, multiple-site optical recording techniques in combination with high-resolution video microscopy were used to image neural activity in rat olfactory bulb slices after electrical stimulation of the olfactory nerve layer. Within the glomerular layer, the presynaptic signal was followed, at short latency, by a large, slow depolarization. Available evidence suggests that this postsynaptic optical response primarily reflects activity in periglomerular cells. The effects of low Cl^- Ringer's solution and bath application of SITS, a Cl^- channel blocker, on the postsynaptic glomerular layer signal can be explained by assuming that peri-

←

Figure 6. Chloride sensitivity of the glomerular layer and external plexiform layer optical signals. *A*, Outline of photodiode array shown superimposed on a photomicrograph of the slice preparation. *Filled grid boxes* indicate recording locations for the olfactory nerve layer (*ONL, white*), glomerular layer (*GLOM, black*), and external plexiform layer (*EPL, white*) signals shown in *B* and *C*. Data presented in *D* and *E* were obtained in different preparations. *B*, *Thin traces* show responses recorded in normal Ringer's solution (control); *thick lines* show responses recorded 25 min after $[Cl^-]_o$ was lowered by replacing NaCl with sodium propionate in the bathing medium ("0 Cl^-"). Note the large increase in the amplitude of the conditioning response recorded in the glomerular layer and external plexiform layer in "0 Cl^-." *C*, Time series showing the progressive effects of lowering the $[Cl^-]_o$. The two sets of traces shown at the *left* in *C* were shown superimposed in *B*. Note that after 30 min exposure, the external plexiform layer is virtually eliminated, whereas the glomerular layer signal is still above control levels. *D*, Superimposed records showing the pretreatment response (*thin traces*) and the post-treatment response (*thick traces*) after bath application of 100 μM BMI and 100 μM PTX for 32 min. *E*, Superimposed records show the pretreatment response (*thin traces*) and the post-treatment response (*thick traces*) after bath application of 1 mM SITS for 32 min. *Dashed line* shows partial recovery of the glomerular layer response after a 60 min wash. *Small boxes* below the x-axes indicate the onset of the conditioning and test pulses. Traces shown in *B*, *C*, and *E* were recorded using a 730 ± 40 nm interference filter. Traces shown in *D* were recorded with a 720 ± 30 nm interference filter.

glomerular cells possessed a voltage-dependent Cl^- conductance that is activated by orthodromic stimulation and a Cl^- equilibrium potential that favors Cl^- efflux.

REFERENCES

Adrian ED (1950) The electrical activity of the mammalian olfactory bulb. Electroencephalogr Clin Neurophysiol 2:377–388.

Allison AC, Warwick TT (1949) Quantitative observations on the olfactory system of the rabbit. Brain 72:186–197.

Cinelli AR, Kauer JS (1992) Voltage-sensitive dyes and functional activity in the olfactory pathway. Annu Rev Neurosci 15:321–351.

Cinelli AR, Salzberg BM (1990) Multiple site optical recording of transmembrane voltage (MSORTV), single-unit recordings, and evoked field potentials from the olfactory bulbs of skate (*Raja erinacea*). J Neurophysiol 64:1767–1790.

Cinelli AR, Salzberg BM (1992) Dendritic origin of late events in optical recordings from salamander olfactory bulb. J Neurophysiol 68:786–806.

Dubin AE, Dionne VE (1994) Action potentials and chemosensitive conductances in the dendrites of olfactory neurons suggest new features for odor transduction. J Gen Physiol 103:181–201.

Duclaux R, Mei N, Ranieri F (1976) Conduction velocity along the afferent vagal dendrites: a new type of fibre. J Physiol (Lond) 260:487–495.

Farbman AI (1992) Cell biology of olfaction. Cambridge: Cambridge UP.

Freeman WJ (1974a) Attenuation of transmission through glomeruli of olfactory bulb on paired pulse shock stimulation. Brain Res 65:77–90.

Freeman WJ (1974b) Relation of glomerular neuronal activity to glomerular transmission attenuation. Brain Res 65:91–107.

Getchell TV, Shepherd GM (1975a) Synaptic action on mitral and tufted cells elicited by olfactory nerve volleys in the rabbit. J Physiol (Lond) 251:497–522.

Getchell TV, Shepherd GM (1975b) Short-axon cells in the olfactory bulb: dendrodendritic synaptic interactions. J Physiol (Lond) 251:523–548.

Gray PTA, Ritchie JM (1986) A voltage-gated chloride conductance in rat cultured astrocytes. Proc R Soc Lond [Biol] 228:267–288.

Grinvald A, Frostig RD, Lieke E, Hildesheim R (1988) Optical imaging of neuronal activity. Physiol Rev 68:1285–1366.

Grinvald A, Hildesheim R, Farber IC, Anglister L (1982a) Improved fluorescent probes for the measurement of rapid changes in membrane potential. Biophys J 39:301–388.

Grinvald A, Manker A, Segal M (1982b) Visualization of the spread of electrical activity in rat hippocampal slices by voltage-sensitive optical probes. J Physiol (Lond) 333:269–291.

Hajos F, Gerics B, Sotonyi P (1992) Slices from the rat olfactory bulb maintained in vitro: morphological aspects. J Neurosci Methods 44:225–232.

Hamilton KA, Kauer JS (1988) Responses of mitral/tufted cells to orthodromic and antidromic electrical stimulation in the olfactory bulb of the tiger salamander. J Neurophysiol 59:1736–1755.

Inoue I (1985) Voltage-dependent chloride-conductance of the squid axon membrane and its blockade by disulfonic stilbene derivatives. J Gen Physiol 85:519–537.

Jahr CE, Nicoll RA (1981) Primary afferent depolarization in the in vitro frog olfactory bulb. J Physiol (Lond) 318:375–384.

Kauer JS (1988) Real-time imaging of evoked activity in local circuits of the salamander olfactory bulb. Nature 331:166–168.

Kauer JS, Senseman DM, Cohen LB (1987) Odor-elicited activity monitored simultaneously from 124 regions of the salamander olfactory bulb using a voltage-sensitive dye. Brain Res 418:255–261.

Knauf PA, Rothstein A (1971) Chemical modification of membranes. I. Effect of sulhydryl and amino reactive reagents on anion and cation permeability of the human red blood cell. J Gen Physiol 58:190–210.

Konnerth A, Obaid AL, Salzberg BM (1987) Optical recording of electrical activity from parallel fibres and other cell types in skate cerebellar slices in vitro. J Physiol (Lond) 393:681–702.

Le Gros Clark WE (1951) The projection of the olfactory epithelium on the olfactory bulb of the rabbit. J Neurol Neurosurg Psychiatry 14:1–10.

Mori K, Nowycky MC, Shepherd GM (1981) Analysis of synaptic potentials in mitral cells in the isolated turtle olfactory bulb. J Physiol (Lond) 314:295–309.

Nickell WT, Behbehani MM, Shipley MT (1994) Evidence for $GABA_B$-mediated inhibition of transmission from the olfactory nerve to mitral cells in the rat olfactory bulb. Brain Res Bull 35:119–123.

Nicoll RA (1972) Olfactory nerves and their exciting action in the olfactory bulb. Exp Brain Res 14:185–197.

Nowycky MC, Mori K, Shepherd GM (1981) GABAergic mechanisms of dendrodendritic synapses in isolated turtle olfactory bulb. J Neurophysiol 46:639–648.

Orbach HS, Cohen LB (1983) Optical monitoring of activity from many areas of the in vitro and in vivo salamander olfactory bulb: a new method for studying functional organization in the vertebrate central nervous system. J Neurosci 3:2251–2262.

Orona E, Rainer E, Scott J (1984) Dendritic and axonal organization of mitral and tufted cells in the rat olfactory bulb. J Comp Neurol 226:346–356.

Orrego F (1961) The reptilian forebrain. II. Electrical activity in the olfactory bulb. Arch Ital Biol 99:446–465.

Ottoson D (1959) Olfactory bulb potentials induced by electrical stimulation of the nasal mucosa in the frog. Acta Physiol Scand 47:160–172.

Pinching AJ, Powell TPS (1971a) The neuron types of the glomerular layer of the olfactory bulb. J Cell Sci 9:305–345.

Pinching AJ, Powell TPS (1971b) The neuropil of the glomeruli of the olfactory bulb. J Cell Sci 9:347–377.

Pinching AJ, Powell TPS (1971c) The neuropil of the periglomerular region of the olfactory bulb. J Cell Sci 9:379–409.

Rall W, Shepherd GM (1968) Theoretical reconstruction of field potentials and dendrodendritic synaptic interactions in olfactory bulb. J Neurophysiol 31:884–915.

Schneider SP, Macrides F (1978) Laminar distributions of interneurons in the main olfactory bulb of the adult hamster. Brain Res Bull 3:73–82.

Scott JW, Wellis DP, Riggott MJ, Buonviso N (1993) Functional organization of the main olfactory bulb. Microsc Res Tech 24:142–156.

Senseman DM (1994) NMDA blockade partially reverses paired-pulse depression in the turtle olfactory bulb. Soc Neurosci Abstr 20:1473.

Senseman DM, Rea MA (1994) Fast multisite optical recording of mono- and polysynaptic activity in the hamster suprachiasmatic nucleus evoked by retinohypothalamic tract stimulation. NeuroImage 1:247–263.

Senseman DM, Vasquez S, Nash PL (1990) Animated pseudocolor activity maps (PAM's): scientific visualization of brain electrical activity. In: Chemosensory information processing NATO ASI Series, Vol H39, (Schilds D, ed), pp 329–347. Berlin: Springer.

Shepherd GM (1979) The synaptic organization of the brain. pp 152–183. New York: Oxford UP.

Shepherd GM (1990) The synaptic organization of the brain, 3rd Ed, pp 133–169. New York: Oxford UP.

Siklos L, Rickmann M, Joo F, Freeman WJ, Wolff JR (1995) Chloride is preferentially accumulated in a subpopulation of dendrites and periglomerular cells of the main olfactory bulb in adult rats. Neuroscience 64:165–172.

Solis JL, Nickell WT, Senseman DM (1993) Optical recording of evoked neural activity in rat olfactory bulb slices. Soc Neurosci Abstr 19:122.

Waldrow U, Nowycky MC, Shepherd GM (1981) Evoked potential and single unit responses to olfactory nerve volleys in the isolated turtle olfactory bulb. Brain Res 211:267–283.

Wellis DP, Kauer JS (1993) $GABA_A$ and glutamate receptor involvement in dendrodendritic synaptic interactions from the salamander olfactory bulb. J Physiol (Lond) 469:315–339.

Wellis DP, Scott JW (1990) Intracellular responses of identified rat olfactory bulb interneurons to electrical and odor stimulation. J Neurophysiol 64:932–947.

Wu J-Y, Cohen LB (1993) Fast multisite optical measurement of membrane potential. In: Fluorescent and luminescent probes for biological activity (Mason WT, ed), pp 389–404. New York: Academic.